IEEE Access
Multidisciplinary : Rapid Review : Open Access Journal

Received June 3, 2020, accepted June 11, 2020, date of publication June 15, 2020, date of current version June 24, 2020.

Digital Object Identifier 10.1109/ACCESS.2020.3002608

Recurrent Neural Network for State Adjustment of Redundant Manipulators

LONG JIN[1,2], (Member, IEEE), LI HE[2], ZHIGUAN HUANG[1], AND JUN WANG[3]
[1]Guangdong Provincial Engineering Technology Research Center for Sports Assistive Device, Guangzhou Sport University, Guangzhou 510000, China
[2]School of Information Science and Engineering, Lanzhou University, Lanzhou 730000, China
[3]Gansu Institute of Food Inspection and Research, Lanzhou 730000, China

Corresponding authors: Long Jin (longjin@ieee.org) and Zhiguan Huang (zhiguan1980@163.com)

This work was supported in part by the National Natural Science Foundation of China under Grant 61703189, in part by the Guangzhou Sport University Innovation and Strengthen Project under Grant 5200080589, in part by the Ministry of Education Industry-Academic Cooperation Collaborative Education Program of China under Grant 201901007048, in part by Baidu Online Network Technology (Beijing) Company Ltd., in part by the Team Project of Natural Science Foundation of Qinghai Province, China, under Grant 2020-ZJ-903, in part by the Key Laboratory of IoT of Qinghai under Grant 2020-ZJ-Y16, in part by the Fundamental Research Funds for the Central Universities under Grant lzujbky-2019-89, in part by the National Key Research and Development Program of China under Grant 2017YFE0118900, and in part by the Natural Science Foundation of Gansu Province, China, under Grant 18JR3RA264.

ABSTRACT To make joints of a redundant manipulator moving automatically to a target state, a state-adjustment (SA) scheme is studied and modified in this paper. Specifically, owing to the problem of non-zero initial joint velocity in the SA scheme leading to a potential hazard to redundant manipulators, a modified state-adjustment (MSA) scheme is obtained on the basis of the SA scheme. The MSA scheme achieves the state adjustment by minimizing the differences between the joint angles and the target values. For solving the MSA scheme, a recurrent neural network (RNN) model is derived, of which the critical component is to iterate over the joint angles and joint velocities. The MSA scheme solved by the RNN model enables the redundant manipulator to adjust to the target state automatically while ensuring that the initial joint velocity is zero. Beyond that, several comparative simulations demonstrate the availability and accuracy of the MSA scheme solved by the RNN model in controlling the state adjustment of redundant manipulators.

INDEX TERMS State-adjustment scheme, recurrent neural network, redundant manipulators.

I. INTRODUCTION

Recently, with the gradual maturity of robot technology, manipulators have become a common tool in industrial production and other fields [1]–[3]. A manipulator with more degrees of freedom than required to complete tasks is called a redundant manipulator. Compared with non-redundant manipulators, redundant manipulators are more flexible, which provides the possibility of controlling the pose and avoiding obstacles when executing tasks [4]–[6]. Therefore, in recent years, redundant manipulators have received considerable attention, and studies on the motion control and applications of redundant manipulators have emerged in an endless stream [7]–[11]. For example, Xie *et al.* exploit data-driven technology to fulfill the flexible performance of redundant manipulators and present a high-performance repetitive motion scheme [10]. Besides, the control approach is extended to the acceleration level with the quantitative relationship between the joint space error and Cartesian space error explored [11].

The redundancy solution scheme is the method to obtain the optimal joint angles referring to the optimization index when the target trajectory of the end-effector is known [12], [13]. The optimization technique, especially quadratic programming, is a common technique in the redundancy solution problem. Generally speaking, when performing a redundancy solution, the redundancy solution problem would be transformed into an optimization problem and solved by numerical algorithms (e.g., Newton iteration, gradient-related methods, neural networks) [14]. The Newton iteration and its related improvement methods can make the system converge to the theoretical solution, but some of them are only applicable to the solution of static problems [15]. For the problem of redundancy resolution which needs to be solved dynamically, these methods bring about the time-delay problem due to the absence of leveraging the time derivatives of dynamic parameters. Neural networks, with universal approximation property [16], fault-tolerance [17], parallelism [18], and

The associate editor coordinating the review of this manuscript and approving it for publication was Xiaosong Hu.

excellent learning capabilities [19], are widely applied to address all kinds of complicated problems [20]. Recurrent neural networks (RNNs) have natural advantages in solving real-time problems because they contain hidden layers that can store data from the past, which is conducive to subsequent computations [21]. To date, numerous RNNs have been exploited to solve dynamic optimization problems converted from robotics [22]–[25]. For instance, in [24], a neural algorithm with an estimation on Hessian matrix inversion, as a special kind of RNN, is presented to solve the dynamic unconstrained optimization problem. Besides, a discrete-time neural dynamics model is further investigated in [25] for handling complex-valued quadratic programming problems with equality constraints and applied to robot motion generation.

State adjustment refers to the process of moving the manipulator from the current state to the target state [26] without the displacement of the end-effector. Most of the research on the redundant manipulator focuses on motion planning such as the manipulability optimization method stated in [27] during the task execution of the redundant manipulator, but there are few achievements on the problem of state adjustment [28]–[30]. In fact, state adjustment is imperative in certain situations [31], [32]. For instance, some tasks require the initial pose of the manipulator to be in a specific state, and thus the manipulator needs to be adjusted to the specific state for performing subsequent operations [33], [34]. Moreover, during the execution of repetitive motion, the joint drift phenomenon happens occasionally, which means that the joints of the manipulator fail to return to their original states for a completed task cycle [35], [36]. Considering the problems described above, a state-adjustment (SA) scheme based on the perspective of kinematics is studied and modified, which allows joint angles to converge to target values with high precision automatically. Owing to the SA scheme failing to guarantee zero initial joint velocity, this paper further investigates a modified state-adjustment (MSA) scheme that is exactly right to handle the problem of non-zero initial joint velocity, and then an RNN is proposed to solve this MSA scheme. Eventually, the validity and accuracy of the redundant manipulator synthesized by the MSA scheme solved by the RNN model for moving from the initial state to the target state are illustrated by simulations.

The remainder of the paper is divided into the following sections. In Section II, the SA scheme for redundant manipulators is firstly discussed, and then an MSA scheme is explored as an improvement. As described in Section III, an RNN model is derived to solve the MSA scheme, and its convergence is presented as well. In Section IV, comparative simulations are carried out to examine the effectiveness of the MSA scheme solved by the RNN. Section V concludes this paper. Before ending the current section, the main contributions of the paper are generalized as follows:

1) The MSA scheme researched in this paper is able to make the redundant manipulator move from one state to the target state via decreasing the difference between the joint angle and the target state without the displacement of the end-effector. Considering the physical realizability, the MSA scheme exploits and modifies the constraint of joint velocity to obtain the zero initial joint velocity.
2) An RNN is proposed to solve the MSA scheme at the velocity level with the proof on its global convergence displayed. The simulations based on Cartesian three-dimensional space under different parameter setting conditions verify the validity and accuracy of the MSA scheme solved by the RNN model. Besides, the influence of parameters on the convergence speed and accuracy is explored through comparison simulation.

II. SA SCHEME AND MSA SCHEME

In this section, an MSA scheme with zero initial joint velocity is studied to adjust the pose of the redundant manipulator to the target state based on the SA scheme.

A. SA SCHEME

Before the research on the SA scheme, the essential kinematic equations of the redundant manipulator is explained. Assume that the number of joints of the redundant manipulator is m and the joint angle is $\sigma(t) = [\sigma_1, \sigma_2, \cdots, \sigma_m]^{\mathrm{T}} \in \mathbb{R}^m$ with the superscript $^{\mathrm{T}}$ denoting the transpose operator. By defining $f(\cdot)$ as the mapping between the joint angles and position of the end-effector of the redundant manipulator, the position $p_{\mathrm{e}} \in \mathbb{R}^k$ is expressed as $p_{\mathrm{e}} = f(\sigma(t))$, and the velocity of the end-effector $\dot{p}_{\mathrm{e}}$ is written as

$$\dot{p}_e = J\dot{\sigma}(t), \tag{1}$$

where $J = \partial f(\sigma(t))/\partial\sigma(t) \in \mathbb{R}^{k\times m}$, and $\dot{\sigma}(t)$ is the joint velocity. In addition, suppose that the initial state or current state of the redundant manipulator is $\sigma(0) \in \mathbb{R}^m$, and the target state is $\sigma_{\mathrm{s}} \in \mathbb{R}^m$. The ultimate goal of the designed SA scheme is $\sigma(t) = \sigma_{\mathrm{s}}$, that is, each joint angle of the redundant manipulator should change into the target value.

According to the above explanations, the SA scheme is constructed as

$$\begin{aligned} &\min\ \frac{1}{2}\dot{\sigma}^{\mathrm{T}}(t)\dot{\sigma}(t) + \varrho^{\mathrm{T}}(t)\dot{\sigma}(t)\\ &\text{s.t. } J\dot{\sigma}(t) = \dot{p}_{\mathrm{e}}\\ &\qquad \sigma^- \leq \sigma(t) \leq \sigma^+\\ &\qquad \dot{\sigma}^- \leq \dot{\sigma}(t) \leq \dot{\sigma}^+, \end{aligned} \tag{2}$$

where $\varrho(t) = r(\sigma(t) - \sigma_{\mathrm{s}}) \in \mathbb{R}^m$; $r > 0$; $\dot{\sigma}(t) = \mathrm{d}\sigma(t)/\mathrm{d}t$ is the real-time joint velocity; $\sigma^{\mp}$ and $\dot{\sigma}^{\mp}$ are the lower and upper bound limits of the joint angle and joint velocity separately. Note that, the position of the end-effector remains unchanged during the state adjustment task, resulting in $\dot{p}_{\mathrm{e}} = \mathbf{0}$. In SA scheme (2), the objective function can realize the pose adjustment of the redundant manipulator, and its constraint conditions can guarantee that $\dot{\sigma}(t)$ and $\sigma(t)$ are kept within the constraint range.

The following remark focuses on explaining the intrinsic consistency between the minimized objective function and the expected result $\sigma(t) = \sigma_{\mathrm{s}}$.

Remark 1: In the SA scheme (2), the redundant robot manipulator can automatically approach the target state by minimizing $\dot{\sigma}^{\mathrm{T}}(t)\dot{\sigma}(t)/2+\varrho^{\mathrm{T}}(t)\dot{\sigma}(t)$.

The derivation of the minimization index $\dot{\sigma}^{\mathrm{T}}(t)\dot{\sigma}(t)/2+\varrho^{\mathrm{T}}(t)\dot{\sigma}(t)$ is explained in detail next. First, make the following definitions:

$$\mathbf{e}(t)=\sigma(t)-\sigma_{\mathrm{s}}, \tag{3}$$

and

$$\dot{\mathbf{e}}(t)=-r\mathbf{e}(t), \tag{4}$$

where $\mathbf{e}(t)\in\mathbb{R}^m$ denotes the error between the joint angle and the target state, and $\dot{\mathbf{e}}(t)=\mathrm{d}\mathbf{e}(t)/\mathrm{d}t$ is its derivative. The solution to differential equation (4) is

$$\mathbf{e}(t)=\mathbf{e}(0)\exp(-rt), \tag{5}$$

where $\mathbf{e}(0)=\sigma(0)-\sigma_{\mathrm{s}}$ is the initial angle error. As observed from (5), $\mathbf{e}(t)$ converges exponentially to zero and r can adjust the convergence rate. Thanks to the convergence of $\mathbf{e}(t)$, the final state of the redundant manipulator can be consistent with the target state if there is sufficient adjustment time. Secondly, the combination of (3) and (4) brings about

$$\dot{\sigma}(t)+r(\sigma(t)-\sigma_{\mathrm{s}})=\mathbf{0}. \tag{6}$$

The above analysis can be summarized that, the joint angle can exponentially converge to σ_{s} as long as (6) is satisfied. Hence, the state adjustment of a redundant manipulator can be carried out by minimizing $\dot{\sigma}(t)+r(\sigma(t)-\sigma_{\mathrm{s}})$. Due to the hidden demands in the redundant manipulator's task, it is $\|\dot{\sigma}(t)+r(\sigma(t)-\sigma_{\mathrm{s}})\|_2^2$ more appropriate in physical operations rather than $\dot{\sigma}(t)+r(\sigma(t)-\sigma_{\mathrm{s}})$, where $\|\cdot\|_2$ is the operator to obtain the two-norm of a vector. Expand $\|\dot{\sigma}(t)+r(\sigma(t)-\sigma_{\mathrm{s}})\|_2^2$ and define $\varrho(t)=r(\sigma(t)-\sigma_{\mathrm{s}})$ to get

$$\begin{aligned}&\|\dot{\sigma}(t)+r(\sigma(t)-\sigma_{\mathrm{s}})\|_2^2\\&\quad=\dot{\sigma}^{\mathrm{T}}(t)\dot{\sigma}(t)+2\varrho^{\mathrm{T}}(t)\dot{\sigma}(t)+\varrho^{\mathrm{T}}(t)\varrho(t).\end{aligned} \tag{7}$$

In terms of the velocity level, $\varrho^{\mathrm{T}}(t)\varrho(t)$ is a constant. Eventually, the minimum index of the SA scheme (2) is described as $\dot{\sigma}^{\mathrm{T}}(t)\dot{\sigma}(t)/2+\varrho^{\mathrm{T}}(t)\dot{\sigma}(t)$, with ignoring the performance of $\varrho^{\mathrm{T}}(t)\varrho(t)$.

B. MSA SCHEME

In the task of solving real-time joint velocities, it is a complicated thing to constrain joint angles, and thus, two different levels of joint physical constraints in SA scheme (2) should be written as a comprehensive constraint. The new bounds of the joint velocity are redefined as $\psi^{\mp}$, and the new upper and lower limits of the jth joint velocity are expressed as

$$\begin{aligned}\psi_j^+&=\min\{\dot{\sigma}_j^+,\lambda(\sigma_j^+-\sigma_j)\}\\ \psi_j^-&=\max\{\dot{\sigma}_j^-,\lambda(\sigma_j^--\sigma_j)\},\end{aligned} \tag{8}$$

where $\dot{\sigma}_j^+$ and σ_j^+ are the upper limits of the jth joint velocity and angle; $\dot{\sigma}_j^-$ and σ_j^- are the lower limits of jth joint velocity and angle; $\lambda>0$ is the scale factor. In (8), once the joint angle is too large, the inherent upper limit of joint velocity would be replaced by $\lambda(\sigma_j^+-\sigma_j)$, which drives the joint angle to change into the constraint range. Similarly, when the joint angle is too small, $\lambda(\sigma_j^--\sigma_j)$ would replace the inherent lower limit of joint velocity, avoiding the joint velocities out of the constraint range. In this way, the range of joint velocities can be controlled while the range of joint angles can be constrained. Note that, in this subsection and subsequent derivations, these time-varying variables are simplified such as σ for $\sigma(t)$.

Aided with the preparatory work above, SA scheme (2) is simplified as

$$\begin{aligned}&\min\ \frac{1}{2}\omega^{\mathrm{T}}\omega+\varrho^{\mathrm{T}}\omega\\&\text{s.t. } J\omega=\dot{p}_{\mathrm{e}}\\&\qquad\psi^-\le\omega\le\psi^+,\end{aligned} \tag{9}$$

where $\omega=\dot{\sigma}\in\mathbb{R}^m$. Formally, SA scheme (2) is simplified as a quadratic optimization scheme at the velocity level, which only contains a range constraint and is easier to solve, in contrast to SA scheme (2).

The SA scheme (2) generally leads to a phenomenon that the initial joint velocity is not zero with the influence of $\omega(0)=-r(\sigma(0)-\sigma_{\mathrm{s}})$. In practice, the joint velocity of the redundant manipulator maintains zero at the beginning of the movement, and then gradually increases. If there is a large joint velocity at the initial state, the damage to the redundant manipulator is self-evident. Therefore, the following improvements are added to get the MSA scheme:

$$\begin{aligned}&\min\ \frac{1}{2}\omega^{\mathrm{T}}\omega+\varrho^{\mathrm{T}}\omega\\&\text{s.t. } J\omega=\dot{p}_{\mathrm{e}}\\&\qquad\Psi^-\le\omega\le\Psi^+,\end{aligned} \tag{10}$$

where Ψ^- and Ψ^+ are the modified lower and upper bounds of the joint velocity. Specifically, Ψ^- and Ψ^+ are defined as

$$\begin{aligned}\Psi^-&=\sin(\pi t/2T)\psi^-\\ \Psi^+&=\sin(\pi t/2T)\psi^+,\end{aligned} \tag{11}$$

where T is the stipulated state-adjustment time. Compared with (8), a time-varying sine function is added to the constraint as a multiplier, which enables the limits of joint velocity to expand gradually during the motion, makes the joint velocity to increase from zero and avoids the problem of excessive initial joint velocity. Hence, through this method, MSA scheme (10) possesses the merit of zero initial joint velocity and becomes more safe and reliable than SA scheme (2).

III. SOLUTION

To obtain joint velocity data that can control the motion of redundant manipulator, developing a corresponding solver to solve MSA scheme (10) is indispensable. The following content is the derivation procedure of the effective RNN model solver.

First, based on MSA scheme (10), a Lagrangian function is defined as $F(\omega) = \omega^{\mathrm{T}}\omega/2 + \varrho^{\mathrm{T}}\omega + \gamma^{\mathrm{T}}J\omega$, with $\gamma \in \mathbb{R}^k$ denoting the Lagrange-multiplier vector. As known from the Karush-Kuhn-Tucker condition [37], the optimal solution to MSA scheme (10) satisfies

$$\begin{aligned} N_{\Psi}(\omega) + \frac{\partial F}{\partial \omega} &\ni \mathbf{0}, \\ J\omega &= \mathbf{0}, \end{aligned} \tag{12}$$

where $N_{\Psi}(\omega)$ is the normal cone of set Ψ at ω and satisfies

$$(\eta - \omega)^{\mathrm{T}}(\frac{\partial F}{\partial \omega}) \geq 0, \ \ \forall \eta \in \Psi. \tag{13}$$

Preform the following operations to get

$$\begin{aligned} &\|\eta - (\omega - \frac{\partial F}{\partial \omega})\|_2^2 - \|\omega - (\omega - \frac{\partial F}{\partial \omega})\|_2^2 \\ &\quad = \|\omega - \eta\|_2^2 + 2(\eta - \omega)^{\mathrm{T}}(\frac{\partial F}{\partial \omega}) \geq 0. \end{aligned} \tag{14}$$

Then, (12) is reformulated into

$$\omega = \Gamma_{\Psi}(\omega - \frac{\partial F}{\partial \omega}) = \Gamma_{\Psi}(-\varrho - J^{\mathrm{T}}\gamma), \tag{15}$$

where the projection function $\Gamma_{\Psi}(\cdot)$ is defined as

$$\Gamma_{\Psi}(a) = \arg\min \|h - a\|_2^2, \ \ \forall h \in \Psi \tag{16}$$

with $\mathbf{0} \in \Psi$ and is equivalent to

$$\begin{aligned} \Gamma_{\Psi}(a) = b, \ \text{with} \ \|h - a\|_2^2 - \|b - a\|_2^2 \geq 0, \\ b \in \Psi, \ \forall h \in \Psi. \end{aligned} \tag{17}$$

Finally, to solve equation (15), an RNN is exploited and written as a differential equation:

$$\begin{aligned} \epsilon\dot{\omega} &= -\omega + \Gamma_{\Psi}(-\varrho - J^{\mathrm{T}}\gamma), \\ \epsilon\dot{\gamma} &= J\omega, \end{aligned} \tag{18}$$

where $\epsilon > 0$ is the proportional coefficient.

Facilitated by the same derivation method, the corresponding RNN exploited for the SA scheme (2) is described as follows:

$$\begin{aligned} \epsilon\dot{\omega} &= -\omega + \Gamma_{\psi}(-\varrho - J^{\mathrm{T}}\gamma), \\ \epsilon\dot{\gamma} &= J\omega, \end{aligned} \tag{19}$$

where the definition of nonlinear projection function $\Gamma_{\psi}(\cdot)$ is the same as (16), except that Ψ is replaced by ψ. Note that RNN model (19) is different from RNN (18) although they are similar except for the individual parameter. Besides, the RNN model (18) is applied to solve MSA scheme (10), and the other is used for solving SA scheme (2).

The following theorem illustrates the convergence of RNN model (18) in solving MSA scheme (10).

Theorem 1: The output of proposed RNN model (18) for solving MSA scheme (10) converges to its optimal solution.

Proof: First, by defining $\rho = [\omega, \gamma]^{\mathrm{T}} \in \Omega$ with $\Omega = \{[\omega, \gamma]^{\mathrm{T}} \in \mathbb{R}^{k+m} | \omega \in \Psi, \gamma \in \mathbb{R}^k\}$, (18) is rewritten as

$$\epsilon\dot{\rho} = -\rho + \Gamma_{\Omega}(\rho - G(\rho)), \tag{20}$$

where the function $G(\rho)$ is defined as

$$G(\rho) = \begin{bmatrix} \omega + \varrho + J^{\mathrm{T}}\gamma \\ -J\omega \end{bmatrix} \in \mathbb{R}^{m+k}, \tag{21}$$

and its gradient is

$$\nabla G = \begin{bmatrix} I & J^{\mathrm{T}} \\ -J & 0 \end{bmatrix} \in \mathbb{R}^{k+m \times k+m}, \tag{22}$$

with I standing for an identity matrix, and ∇ being the symbol for the gradient. Then, the monotonicity of $G(\omega)$ is inferred from

$$\begin{aligned} &(\rho_1 - \rho_2)^{\mathrm{T}}(G(\rho_1) - G(\rho_2)) \\ &\quad = (\rho_1 - \rho_2)^{\mathrm{T}}\nabla G(\varsigma)(\rho_1 - \rho_2) \\ &\quad = (\rho_1 - \rho_2)^{\mathrm{T}}(\nabla G(\varsigma) + \nabla^{\mathrm{T}}G(\varsigma))(\rho_1 - \rho_2) \geq 0, \end{aligned} \tag{23}$$

where ρ_1 and ρ_2 are two arbitrary vectors in set Ω, and $\varsigma \in \Omega$ is a vector between ρ_1 and ρ_2. Facilitated by these derivations and lemmas in [38], RNN model (18) is Lyapunov stable and its equilibrium point ρ' conforms to the following variational inequality:

$$(\rho - \rho')^{\mathrm{T}}G(\rho') \geq 0, \ \ \rho \in \Omega. \tag{24}$$

According to the properties of variational inequalities, (24) can also be converted into the following equation:

$$-\rho' + \Gamma_{\Omega}(\rho' - G(\rho')) = \mathbf{0}. \tag{25}$$

The above projection equation has the same solution of (20), which indicates that the output of RNN model (18) converges to the optimal solution of MSA scheme (10). The proof is complete. □

IV. SIMULATION

In current part, for verifying the effectiveness and reliability of the MSA scheme (10) solved by RNN model (18), a series of simulations are carried out.

A. SIMULATION SETTING

Simulations are based on the redundant manipulator KUKA with seven degrees of freedom, and the joint physical limits are as follows: the upper and lower limits of the first, third, fifth and seventh joint angles are $17/18\pi$ and $-17/18\pi$ rad separately; the upper and lower limits for the second, fourth, and sixth joint angles are $2/3\pi$ and $-2/3\pi$ rad separately; the upper and lower limits of each joint velocity are 1.5 and -1.5 rad/s, respectively. Suppose that the initial states of each joint angle are 0.981028, -0.980346, 0.283290, 0.803084, -1.557347, -2.059395, and 1.070796 rad, and the target states are $\pi/4$, $-\pi/4$, $\pi/6$, $\pi/3$, $-\pi/3$, $-\pi/2$, and $\pi/2$ rad. Moreover, the scale factor λ is 20 and the proportion coefficient ϵ is 0.001. Simulations consist of two parts: the first part is the simulation of SA scheme (2) solved by RNN model (19); the second part includes the simulations of the MSA scheme (10) solved by RNN model (18) under different parameter settings.

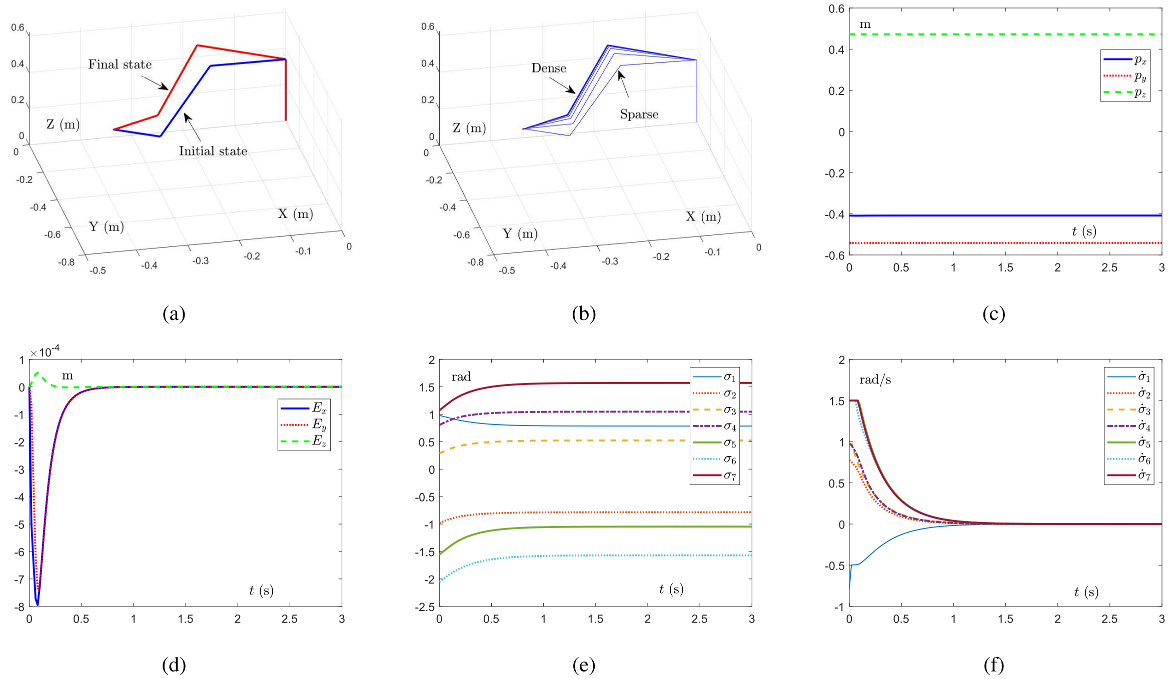

(a) (b) (c)

(d) (e) (f)

FIGURE 1. Simulation results of the redundant manipulator synthesized by SA scheme (2) solved by RNN model (19) with $T = 3$ s and $r = 4$. (a) The initial state and final state. (b) Motion trajectory. (c) Position of the end-effector. (d) Profiles of position errors. (e) Profiles of joint angles. (f) Profiles of joint velocities.

B. SIMULATION RESULTS

The simulation of the redundant manipulator synthesized by SA scheme (2) without zero initial joint velocity is carried out with results shown in Fig. 1. More specifically, the initial state and final state are revealed in Fig. 1(a). The motion trajectory during the adjustment can be seen in Fig. 1(b), in which motion trajectories are sparse near the initial state and become dense near the final state. Owing to the same sampling interval between two adjacent trajectories, this phenomenon suggests that the redundant manipulator possesses a large joint velocity at the initial moment and a low joint velocity at the end. Besides, from the position and position errors of the end-effector displayed in Fig. 1(c) and (d), it can be generalized that the end-effector of the manipulator does not change significantly during the state adjustment. Moreover, as observed in Fig. 1(e) and (f), joint angles can converge from the initial values to the target ones and the joint velocities decrease to zero from a very large one, which goes against the reality that the joint velocities are zero at the start of the task. In addition, the joint velocities of the sixth and seventh remain unchanged at 1.5 rad/s for a short time at the beginning, of which the reason is that the two initial joint velocities ($\dot{\sigma}_6(0) \approx 1.95 > 1.5$ rad/s and $\dot{\sigma}_7(0) \approx 2.00 > 1.5$ rad/s) calculated by $\dot{\sigma}(0) = -r(\sigma(0) - \sigma_{\mathrm{s}})$ in Remark 1 exceed their physical constraints and are adjusted to the boundary values 1.5 rad/s.

The rest content is the simulations of the MSA scheme (10) for the state adjustment of the redundant manipulator, which involves three cases with the corresponding parameter settings for each case as follows: case 1) $T = 3$ s and $r = 4$; case 2) $T = 3$ s and $r = 8$; case 3) $T = 5$ s and $r = 4$. The convergence rate and accuracy of the MSA scheme (10) solved by the proposed RNN model (18) are further explored by comparing the simulations under these three cases. In case 1), the initial state, final state, and motion trajectory of the redundant manipulator synthesized by MSA scheme (10) solved by RNN model (18) with $T = 3$ s and $r = 4$ are shown in Fig. 2(a) and (b). Evidently, motion trajectories are dense when approaching the initial state and the final state, and sparse in the middle part, which indicates that the redundant manipulator moves slowly at the beginning and end of the state adjustment, and moves fast during the intermediate process. Furthermore, by observing the position and position errors of the end-effector in Fig. 2(c) and (d), it is found that there is no obvious displacement at the end-effector of the manipulator, which is consistent with the theoretical analysis. Moreover, profiles of joint angles and velocities are displayed in Fig. 2(e) and (f), in which joint angles converge to the target values in 2 s, and joint velocities increase from zero. Compared with the results of SA scheme (2) in Fig. 1(f), MSA scheme (10) can indeed deal with the problem of non-zero initial joint velocity such that it becomes more applicable. In addition, to observe the results of the state adjustment more accurately, joint-angle errors are revealed in Table 1, in which the absolute values of joint errors under case 1) are all less than 4.3503×10^{-5} rad.

For further analysis, simulation of the redundant manipulator synthesized by MSA scheme (10) solved by RNN model (18) under case 2) is conducted and the corresponding results are revealed in Fig. 3. In the simulation, only joint

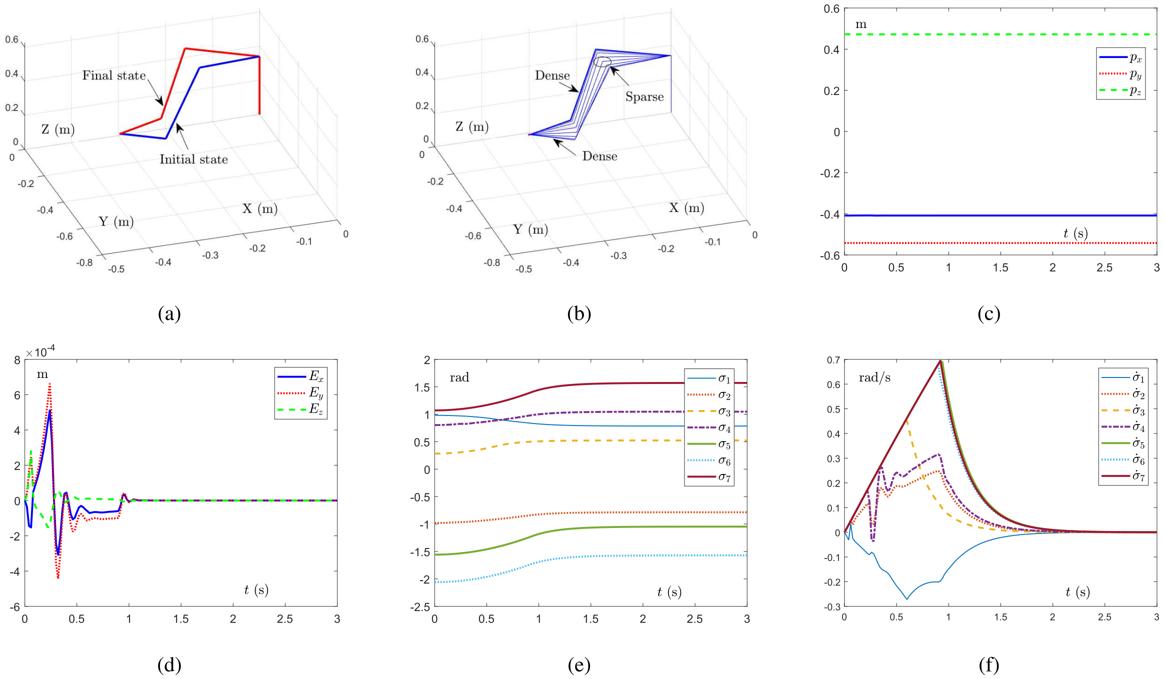

(a) (b) (c)

(d) (e) (f)

FIGURE 2. Simulation results of the redundant manipulator synthesized by MSA scheme (10) solved by RNN model (18) with $T = 3$ s and $r = 4$. (a) The initial state and final state. (b) Motion trajectory. (c) Position of the end-effector. (d) Profiles of position errors. (e) Profiles of joint angles. (f) Profiles of joint velocities.

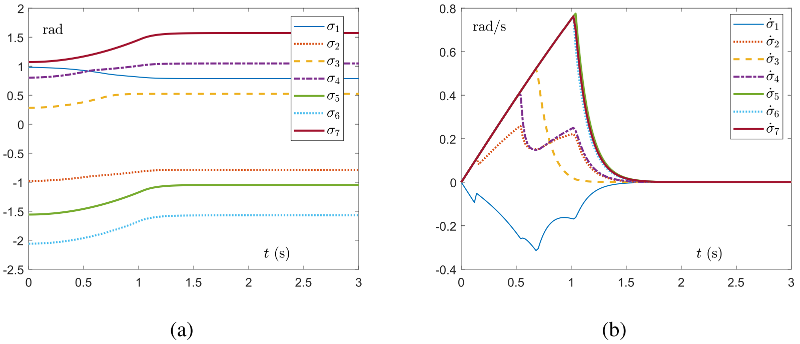

(a) (b)

FIGURE 3. Joint angles and velocities of the redundant manipulator synthesized by MSA scheme (10) solved by RNN model (18) with $T = 3$ s and $r = 8$. (a) Profiles of joint angles. (b) Profiles of joint velocities.

angles and velocities are analyzed, because other simulation results are almost the same as those under case 1) in Fig. 2. By observing the joint angles in Fig. 3(a), it is found that joint angles converge to the target values in 1.5 s, which indicates that the convergence rate of joint angles is improved when r is increased. Furthermore, joint velocities in Fig. 3(b) gradually increase from zero at the beginning and drop to zero around 1.5 s. To explore the change of accuracy with the increase of r, the errors of joint angles are calculated and shown in Table 2, in which the maximum of the absolute value of the error is less than 2.35×10^{-7} rad. In contrast to errors in Table 1, the accuracy is almost a hundred times better, which implies that the accuracy can be improved by increasing r.

As for case 3), joint angles and velocities of the redundant manipulator synthesized by MSA scheme (10) solved by RNN model (18) are shown in Fig. 4. Increasing the task time to 5 s, joint angles in Fig. 4(a) still converge to the target value in 2 s, and joint velocities in Fig. 4(b) drop to zero around 2 s, which indicates that the increase of task time does not affect the convergence rate of joint angles. For exploring the impact of task time on the accuracy, the errors of joint angles are calculated and revealed in Table 3, in which the absolute

TABLE 1. Angle error by applying RNN (18) under Case 1.

$\sigma(0)$	σ_s	$\sigma(T)$	$\lvert\sigma(T)-\sigma_s\rvert$
$+0.981028$	$+\pi/4$	$+0.785411$	1.289461×10^{-5}
-0.980346	$-\pi/4$	-0.785409	1.177066×10^{-5}
$+0.283290$	$+\pi/6$	$+0.523593$	4.891301×10^{-6}
$+0.803084$	$+\pi/3$	$+1.047182$	1.499467×10^{-5}
-1.557347	$-\pi/3$	-1.047241	4.350270×10^{-5}
-2.059395	$-\pi/2$	-1.570835	3.934844×10^{-5}
$+1.070796$	$+\pi/2$	$+1.570755$	4.115238×10^{-5}

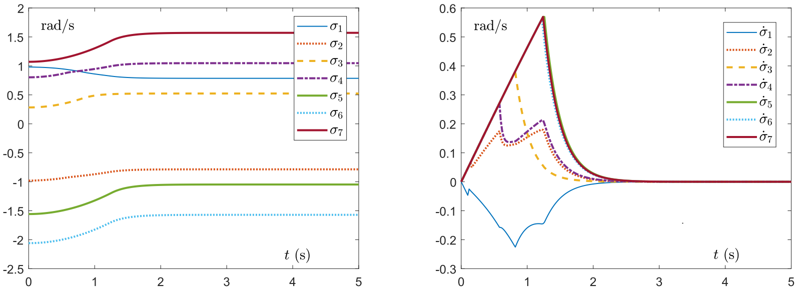

(a)

(b)

FIGURE 4. Joint angles and velocities of the redundant manipulator synthesized by MSA scheme (10) solved by RNN model (18) with $T = 5$ s and $r = 4$. (a) Profiles of joint angles. (b) Profiles of joint velocities.

TABLE 2. Angle Error by Applying RNN (18) under Case 2.

$\sigma(0)$	σ_s	$\sigma(T)$	$\lvert\sigma(T) - \sigma_s\rvert$
$+0.981028$	$+\pi/4$	$+0.785398$	5.007557×10^{-8}
-0.980346	$-\pi/4$	-0.785398	9.679112×10^{-8}
$+0.283290$	$+\pi/6$	$+0.523598$	3.814844×10^{-8}
$+0.803084$	$+\pi/3$	$+1.047197$	2.349258×10^{-7}
-1.557347	$-\pi/3$	-1.047197	9.339705×10^{-9}
-2.059395	$-\pi/2$	-1.570796	1.783016×10^{-7}
$+1.070796$	$+\pi/2$	$+1.570796$	1.185032×10^{-8}

TABLE 3. Angle Error by Applying RNN (18) under Case 3.

$\sigma(0)$	σ_s	$\sigma(T)$	$\lvert\sigma(T) - \sigma_s\rvert$
$+0.981028$	$+\pi/4$	$+0.785398$	4.607877×10^{-8}
-0.980346	$-\pi/4$	-0.785398	9.687483×10^{-8}
$+0.283290$	$+\pi/6$	$+0.523598$	3.839616×10^{-8}
$+0.803084$	$+\pi/3$	$+1.047197$	2.433062×10^{-7}
-1.557347	$-\pi/3$	-1.047197	1.861330×10^{-8}
-2.059395	$-\pi/2$	-1.570796	2.174961×10^{-7}
$+1.070796$	$+\pi/2$	$+1.570796$	3.950501×10^{-8}

values of the error are all almost a hundred times lower than those obtained under case 1). It can be summarized from simulation results under case 3) that changing the task time T improves the accuracy but does not change the convergence rate.

In conclusion, MSA scheme (10) solved by RNN model (18) can solve the problem of non-zero initial joint velocity during the state adjustment, which can change the convergence rate by modifying r, and achieve the desired accuracy by adjusting r and T.

V. CONCLUSION

In this paper, for controlling state adjustment of redundant manipulators, based on the modification of the SA scheme, an MSA scheme has been discussed, which can deal with the non-zero initial joint velocity. To be specific, the MSA scheme concentrates on minimizing the deviations between joint angles and target values, and its constraints include the joint angle constraints and joint velocity constraints. Besides, a sine function multiplier has been added to constrain the initial joint velocity on the basis of the joint limits, which is different from the SA scheme. Further, RNN models have been proposed to solve the SA scheme and the MSA scheme separately. Eventually, the comparative simulation results have elucidated that the MSA scheme with the assistance of the proposed RNN model can remedy the problem of the non-zero initial joint velocity and improve the accuracy greatly by modifying related parameters.

REFERENCES

[1] C. Yang, C. Zeng, Y. Cong, N. Wang, and M. Wang, "A learning framework of adaptive manipulative skills from human to robot," *IEEE Trans. Ind. Informat.*, vol. 15, no. 2, pp. 1153–1161, Feb. 2019.

[2] Y. Wang, L. Cheng, Z.-G. Hou, J. Yu, and M. Tan, "Optimal formation of multirobot systems based on a recurrent neural network," *IEEE Trans. Neural Netw. Learn. Syst.*, vol. 27, no. 2, pp. 322–333, Feb. 2016.

[3] Y. Huang, J. Na, G. Gao, X. Wu, and Y. Guo, "Robust adaptive control for vehicle active suspension systems with uncertain dynamics," in *Proc. 34th Chin. Control Conf. (CCC)*, Jul. 2015, pp. 8033–8038.

[4] C. Yang, Y. Jiang, W. He, J. Na, Z. Li, and B. Xu, "Adaptive parameter estimation and control design for robot manipulators with finite-time convergence," *IEEE Trans. Ind. Electron.*, vol. 65, no. 10, pp. 8112–8123, Oct. 2018.

[5] L. Jin, S. Li, L. Xiao, R. Lu, and B. Liao, "Cooperative motion generation in a distributed network of redundant robot manipulators with noises," *IEEE Trans. Syst., Man, Cybern. Syst.*, vol. 48, no. 10, pp. 1715–1724, Oct. 2018.

[6] D. Guo and Y. Zhang, "Acceleration-level inequality-based MAN scheme for obstacle avoidance of redundant robot manipulators," *IEEE Trans. Ind. Electron.*, vol. 61, no. 12, pp. 6903–6914, Dec. 2014.

[7] X. Xiao, L. Wei, D. Fu, J. Yan, and H. Wang, "Noise-suppressing Newton algorithm for kinematic control of robots," *IEEE Access*, early access, Aug. 28, 2019, doi: 10.1109/ACCESS.2019.2937686.

[8] D. Guo, Q. Feng, and J. Cai, "Acceleration-level obstacle-avoidance scheme for motion planning of redundant robot manipulators," *IEEE Access*, vol. 7, pp. 183040–183048, 2019.

[9] H. Zhang, H. Jin, Z. Liu, Y. Liu, Y. Zhu, and J. Zhao, "Real-time kinematic control for redundant manipulators in a time-varying environment: Multiple-dynamic obstacle avoidance and fast tracking of a moving object," *IEEE Trans. Ind. Informat.*, vol. 16, no. 1, pp. 28–41, Jan. 2020.

[10] Z. Xie, L. Jin, X. Luo, S. Li, and X. Xiao, "A data-driven cyclic-motion generation scheme for kinematic control of redundant manipulators," *IEEE Trans. Control Syst. Technol.*, early access, Jan. 15, 2020, doi: 10.1109/TCST.2019.2963017.

[11] L. Jin, Z. Xie, M. Liu, C. Ke, C. Li, and C. Yang, "Novel joint-drift-free scheme at acceleration level for robotic redundancy resolution with tracking error theoretically eliminated," *IEEE/ASME Trans. Mechatronics*, early access, Apr. 30, 2020, doi: 10.1109/TMECH.2020.3001624.

[12] Z. Jia, S. Chen, X. Qu, P. Zhang, and N. Zhong, "Velocity-level tri-criteria optimization scheme for different complex path tracking of redundant manipulators," *IEEE Access*, vol. 7, pp. 64289–64296, 2019.

[13] Z. Jia, X. Qu, S. Chen, N. Zhong, P. Zhang, and F. Ouyang, "Acceleration-level multi-criteria optimization for remedying joint-angle drift of redundant manipulators on complex path tracking," *IEEE Access*, vol. 7, pp. 95716–95724, 2019.

[14] L. Jin, S. Li, and B. Hu, "RNN models for dynamic matrix inversion: A control-theoretical perspective," *IEEE Trans. Ind. Informat.*, vol. 14, no. 1, pp. 189–199, Jan. 2018.

[15] Y. Saad and H. A. van der Vorst, "Iterative solution of linear systems in the 20th century," *J. Comput. Appl. Math.*, vol. 123, nos. 1–2, pp. 1–33, Nov. 2000.

[16] H. Yang and J. Liu, "An adaptive RBF neural network control method for a class of nonlinear systems," *IEEE/CAA J. Automatica Sinica*, vol. 5, no. 2, pp. 457–462, Mar. 2018.

[17] A. Izadbakhsh and M. Masoumi, "FAT-based robust adaptive control of flexible-joint robots: Singular perturbation approach," in *Proc. IEEE Int. Conf. Ind. Technol. (ICIT)*, Mar. 2017, pp. 803–808.

[18] L. Chen, X. Hu, W. Tian, H. Wang, D. Cao, and F.-Y. Wang, "Parallel planning: A new motion planning framework for autonomous driving," *IEEE/CAA J. Automatica Sinica*, vol. 6, no. 1, pp. 236–246, Jan. 2019.

[19] N. Zerari, M. Chemachema, and N. Essounbouli, "Neural network based adaptive tracking control for a class of pure feedback nonlinear systems with input saturation," *IEEE/CAA J. Automatica Sinica*, vol. 6, no. 1, pp. 278–290, Jan. 2019.

[20] M. R. Fajani, A. Izadbakhsh, and A. H. Ghazvinipour, "Recurrent neural network based second order sliding mode control of redundant robot manipulators," in *Proc. IEEE Int. Conf. Ind. Technol. (ICIT)*, Feb. 2018, pp. 298–303.

[21] Y. Qi, L. Jin, H. Li, Y. Li, and M. Liu, "Discrete computational neural dynamics models for solving time-dependent Sylvester equations with applications to robotics and MIMO systems," *IEEE Trans. Ind. Informat.*, early access, Jan. 20, 2020, doi: 10.1109/TII.2020.2966544.

[22] L. Jin, J. Yan, X. Du, X. Xiao, and D. Fu, "RNN for solving time-variant generalized Sylvester equation with applications to robots and acoustic source localization," *IEEE Trans. Ind. Informat.*, early access, Jan. 8, 2020, doi: 10.1109/TII.2020.2964817.

[23] H. Lu, L. Jin, J. Zhang, Z. Sun, S. Li, and Z. Zhang, "New joint-drift-free scheme aided with projected ZNN for motion generation of redundant robot manipulators perturbed by disturbances," *IEEE Trans. Syst., Man, Cybern. Syst.*, early access, Dec. 19, 2019, doi: 10.1109/TSMC.2019.2956961.

[24] L. Wei, L. Jin, C. Yang, K. Chen, and W. Li, "New noise-tolerant neural algorithms for future dynamic nonlinear optimization with estimation on hessian matrix inversion," *IEEE Trans. Syst., Man, Cybern. Syst.*, early access, May 27, 2019, doi: 10.1109/TSMC.2019.2916892.

[25] Y. Qi, L. Jin, Y. Wang, L. Xiao, and J. Zhang, "Complex-valued discrete-time neural dynamics for perturbed time-dependent complex quadratic programming with applications," *IEEE Trans. Neural Netw. Learn. Syst.*, early access, Nov. 8, 2019, doi: 10.1109/TNNLS.2019.2944992.

[26] K. Li and Y. Zhang, "State adjustment of redundant robot manipulator based on quadratic programming," *Neurocomputing*, vol. 30, pp. 477–489, Jul. 2011.

[27] J. Zhang, L. Jin, and L. Cheng, "RNN for perturbed manipulability optimization of manipulators based on a distributed scheme: A game-theoretic perspective," *IEEE Trans. Neural Netw. Learn. Syst.*, early access, Jan. 28, 2020, doi: 10.1109/TNNLS.2020.2963998.

[28] X. Li, Z. Xu, S. Li, H. Wu, and X. Zhou, "Cooperative kinematic control for multiple redundant manipulators under partially known information using recurrent neural network," *IEEE Access*, vol. 8, pp. 40029–40038, 2020, doi: 10.1109/ACCESS.2020.2974248.

[29] Z. Li, F. Xu, Q. Feng, J. Cai, and D. Guo, "The application of ZFD formula to kinematic control of redundant robot manipulators with guaranteed motion precision," *IEEE Access*, vol. 6, pp. 64777–64783, 2018.

[30] J. Yang, L. Chen, Y. Qi, M. Liu, and C. Cui, "Discrete perturbation-immunity neural network for dynamic constrained redundant robot control," *IEEE Access*, vol. 8, pp. 84490–84500, 2020, doi: 10.1109/ACCESS.2020.2991726.

[31] L. Wang and B. Ma, "Self-motion control of redundant manipulators," *Control Decis.*, vol. 18, no. 2, pp. 199–202, 2002.

[32] K. Li and Y. Zhang, "Design and implementation of a zero-initial-velocity self-motion scheme on a six-DOF planar robot manipulator," *Ind. Robot, Int. J.*, vol. 39, no. 4, pp. 401–411, Jun. 2012.

[33] Y. Zhang and J. Wang, "A dual neural network for constrained joint torque optimization of kinematically redundant manipulators," *IEEE Trans. Syst. Man, Cybern. B, Cybern.*, vol. 32, no. 5, pp. 654–662, Oct. 2002.

[34] Y. S. Xia, G. Feng, and J. Wang, "A primal-dual neural network for online resolving constrained kinematic redundancy in robot motion control," *IEEE Trans. Syst. Man, Cybern. B, Cybern.*, vol. 35, no. 1, pp. 54–64, Feb. 2005.

[35] Z. Zhang and Z. Yan, "Hybrid-level joint-drift-free scheme of redundant robot manipulators synthesized by a varying-parameter recurrent neural network," *IEEE Access*, vol. 6, pp. 34967–34975, 2018.

[36] Y. Zhang, Z. Tan, Z. Yang, and X. Lv, "A dual neural network applied to drift-free resolution of five-link planar robot arm," in *Proc. Int. Conf. Inf. Autom.*, Jun. 2008, pp. 1274–1279.

[37] S. Boyd and L. Vandenberghe, *Convex Optimization*, Cambridge, U.K.: Cambridge Univ. Press, 2004.

[38] L. Jin, S. Li, H. M. La, and X. Luo, "Manipulability optimization of redundant manipulators using dynamic neural networks," *IEEE Trans. Ind. Electron.*, vol. 64, no. 6, pp. 4710–4720, Jun. 2017.

LONG JIN (Member, IEEE) received the B.E. degree in automation and the Ph.D. degree in information and communication engineering from Sun Yat-sen University, Guangzhou, China, in 2011 and 2016, respectively. He is currently a Full Professor with the School of Information Science and Engineering, Lanzhou University, Lanzhou, China. Before joining Lanzhou University in 2017, he was a Postdoctoral Fellow with the Department of Computing, The Hong Kong Polytechnic University, Hong Kong. His main research interests include neural networks, robotics, and intelligent information processing.

LI HE received the B.E. degree from Wuhan University, Wuhan, China, in 2017. She is currently pursuing the M.E. degree in communication and information systems with the School of Information Science and Engineering, Lanzhou University, Lanzhou, China. Her main research interests include robotics, neural networks, intelligent information processing, artificial intelligence, and optimization theory.

ZHIGUAN HUANG was born in Changning, Hunan, China, in 1980. He received the Ph.D. degree in human kinesiology from South China Normal University, Guangzhou, China, in 2009. He is currently an Associate Professor with the Engineering Research Center for Sport Assistive Device, Guangzhou Sport University. He has published around 30 articles in various journals and conferences. His current research interests include neural networks, sport biomechanics, and sport engineering.

JUN WANG received the B.S. and M.S. degrees in inorganic chemistry from Northwest Normal University, Lanzhou, China, in 2007 and 2010, respectively. She is currently with the Gansu Institute of Food Inspection and Research. Her research interests include chemistry and signal processing.